Ultrasound therapy of injury site modulates gene and protein expressions in the dorsal root ganglion in a sciatic nerve crush injury rat model

Shixuan Xu, Akira Ito*, Tianshu Wang, Hideki Kawai, Tomoki Aoyama, Hiroshi Kuroki

Department of Motor Function Analysis, Human Health Sciences, Graduate School of Medicine, Kyoto University, Kyoto, Japan

*Corresponding author: Akira Ito

53 Shogoin, Kawahara-cho, Sakyo-ku, Kyoto 606-8507, Japan

Tel: + 81-75-751-3964; Fax: +81-75-751-3964

E-mail: ito.akira.4m@kyoto-u.ac.jp

Abstract

This study aimed to verify the effects of ultrasound on dorsal root ganglion (DRG) neurons at the injury site in a rat model of sciatic nerve crush injury. We evaluated the mRNA expression of neurotrophic and pro-inflammatory factors by quantitative reverse-transcription polymerase chain reaction 7 and 14 days post-injury. We also evaluated the protein levels of brain-derived neurotrophic factor (BDNF) at 7 and 14 days post-injury. Axon regeneration and motor function analyses were performed 21 days after injury to confirm the facilitative effect of ultrasound on nerve regeneration. In the ultrasound group, *BDNF* and interleukin-6 mRNA expressions of the DRG were significantly reduced seven days post-injury. Compared to the sham group, the BDNF protein expression of the DRG in the ultrasound group remained at a higher level 14 days post-injury. Motor function, myelinated fiber density, and myelin sheath thickness in the ultrasound group were significantly higher than the sham group 21 days post-injury. These results indicate that ultrasound therapy at the injury site promotes nerve regeneration and modulates gene and protein expression in the DRG of a rat model of a sciatic nerve crush injury.

Keywords: ultrasound therapy, dorsal root ganglion, peripheral nerve injury, neurotrophic factor, pro-inflammatory factor, nerve regeneration, gene expression, protein expression, motor function

Introduction

Peripheral nerve injury (PNI) can cause motor and sensory dysfunction (Yang et al. 2011) as well as neuropathic pain that may last a lifetime (Deumens et al. 2010). These factors seriously affect patients' daily lives and work.

Crush injury, the main cause of PNI (Taylor et al. 2008), usually leads to axonotmesis, in which the related neuronal axons and myelin sheaths are damaged but the surrounding endoneurium and other supporting structures are partially or completely intact (Seddon 1943; Robinson 2000). After a nerve crush injury, the injured nerve undergoes Wallerian degeneration (Gaudet et al. 2011; Gordon 2020), and injured axons trigger complex multicellular responses (DeFrancesco-Lisowitz et al. 2015). With the participation of Schwann cells and macrophages, substances related to axonal regeneration, including growth factors and cytokines, are regulated (Martini et al. 2008; Gaudet et al. 2011). The distal stump is prepared to regenerate axons, and reactions for axon elongation occur at the proximal stump after growth cone formation (Gaudet et al. 2011). However, nerve repair takes significant time (Scheib and Höke 2013), which may lead to long-term motor dysfunction. Therefore, effective treatments that promote peripheral nerve regeneration and motor function recovery are required.

In recent years, several treatments have been developed to promote nerve regeneration following PNI, such as invasive electrical stimulation and photobiomodulation with laser therapy, which has been proven to promote axonal regeneration after PNI (Modrak et al. 2020). However, owing to the requirement for

invasive procedures or lack of standardization in treatment, the clinical use of implantable electrical devices and photobiomodulation with laser therapy remains difficult. Therefore, there is an urgent need to develop a standardized, non-invasive treatment to promote peripheral nerve regeneration after PNI.

Ultrasound therapy is a non-invasive intervention for soft tissue and bone fractures (ter Haar 2007). Compared with invasive electrical stimulation, ultrasound therapy does not cause additional problems. In our previous study, the optimal standardized ultrasound procedure for the treatment of PNI was identified (Ito et al. 2020), and its ability to promote axon regeneration after PNI has also been confirmed in animal studies (Chen et al. 2010; Ito et al. 2020; Wang et al. 2021). Thus far, ultrasound therapy of the injured site can promote neurotrophic factor expression in the injured site and dorsal root ganglion (DRG) (Chen et al. 2010; Ni et al. 2017) as well as the anti-inflammatory effects (Ito et al. 2020) of Schwann cells and other cell types at the injured site in the sciatic nerve crush injury model. However, the response of neuronal cell bodies to axonal regeneration remains unclear.

A previous study showed that neuronal death occurs after PNI (West et al. 2007). After PNI, the mRNA and protein expressions of brain-derived neurotrophic factor (*BDNF*) in the DRG, the cell bodies of axons, are upregulated in response to neuronal injury (Sanna et al. 2017; Shen et al. 2020). Moreover, endogenous BDNF protein blockade suppresses the enhanced neurite growth induced by sciatic nerve injury in the DRG (Song et al. 2008). This suggests that the increased BDNF levels in the DRG after PNI may

play a key role in nerve regeneration. Additionally, a report showed that ultrasound therapy after sciatic nerve crush injury upregulated the mRNA expression of *BDNF* in the DRG (Ni et al. 2017). Therefore, we hypothesized that ultrasound therapy at the injury site might promote axon regeneration by affecting the molecular responses of neuronal cell bodies in the DRG.

To further explore the mechanism by which ultrasound promotes nerve regeneration and advances the clinical application of therapeutic ultrasound, it is necessary to verify the effects of ultrasound therapy on DRG neurons after PNI. This study aimed to verify the effects of ultrasound on DRG neurons in a rat model of sciatic nerve crush injury.

Materials and Methods

Animals

The study design is illustrated in Figure 1. A total of seventy-eight 12-week-old male Lewis rats (250–300 g each) were used in this experiment. Three rats were housed per cage with sufficient food and water and a 12-hour light/dark cycle to simulate the day and night cycle. Seventy-two rats were randomly assigned to the ultrasound and sham groups (n = 36 each). Samples from the rats in the ultrasound and sham groups (n = 18 per group) underwent reverse transcription quantitative polymerase chain reaction (RT-qPCR) at 7 and 14 days postoperative (n = 9 for each group at each time point).

Twenty rats in the ultrasound group (n = 10) and sham group (n = 10) were used for immunohistochemistry and hematoxylin and eosin staining analyses at different time

points (7 and 14 days) postoperatively (n = 5 for each group at each time point), and the remaining rats in the ultrasound group (n = 8) and sham group (n = 8) were used for motor function evaluations and axon regeneration evaluation at 21 days postoperative. Three rats were used as intact calibration samples for RT-qPCR and three others were used as intact samples for the immunohistochemistry and hematoxylin and eosin staining analysis. This study was approved by the Animal Experiment Committee of Kyoto University, and all experiments were performed in accordance with the guidelines of the Animal Experiment Committee of Kyoto University (approval no. MedKyo21081).

Surgery

A mixed anesthetic (0.15 mg/kg medetomidine, 2 mg/kg midazolam, 2.5 mg/kg butorphanol) was injected intraperitoneally to anesthetize the rats. We used a rat sciatic nerve crush injury model in this study according to a previously reported protocol (Wang et al. 2018). The left sciatic nerve was exposed via a longitudinal, lateral incision. After the nerve was separated from the surrounding tissue, a 2-mm-long section of the nerve was crushed for 10 s using a needle holder (no. 12501-13; Fine Science Tools Inc., North Vancouver, BC, Canada) at the site below the gluteal tuberosity. The proximal end of the injury site was marked with a 9-0 nylon epineural stitch (T06A09N20-25; Bear Medic Corp., Tokyo, Japan), and the muscle and skin were closed with 4-0 nylon sutures (S15G04N-45; Bear Medic Corp.).

Ultrasound protocol

As previously reported (Ito et al. 2020; Wang et al. 2021; Kawai et al. 2022), ultrasound irradiation was performed using an ultrasonic treatment apparatus (UST-770; ITO Co., LTD, Japan). The coupling gel was applied to the skin above the injury site, onto which the ultrasound transducer (effective radiation area, 0.9 mm^2; beam non-uniformity, 2.9) was placed (Figure. 1B). Our previous studies have shown that ultrasound therapy five or more times per week, for 5 min per day, starting the day after the sciatic nerve crush injury, can effectively promote nerve regeneration (Wang et al. 2021; Kawai et al. 2022). Our previous study also demonstrated that 140 mW/cm^2 is the optimal ultrasound intensity to promote nerve regeneration after a sciatic nerve crush injury (Ito et al. 2020). Based on the above studies, we determined the treatment protocol and ultrasound parameters used in this experiment:1-MHz acoustic frequency, 1-kHz repetition frequency, 140 mW/cm^2 spatial average temporal average intensity, and 20% duty cycle, all for 5 min/day. All rats were anesthetized with 2% isoflurane and received ultrasound or sham stimulation (0 mW/cm^2) daily from the first postoperative day until sacrifice.

Hematoxylin and eosin staining

The rats were transcardially perfused with 200 mL of saline and 200 mL of 4% paraformaldehyde, and the L4 and L5 DRG were dissected. After fixation with 4% paraformaldehyde for 24 h and 30% sucrose for 48 h at 4°C, 10-μm-thick longitudinal

cryostat sections were prepared. In each L4 and L5 DRG specimen, one section was taken for every 15 sections, and three sections were taken from each DRG specimen for hematoxylin and eosin staining. Hematoxylin and eosin staining was then performed on L4 and L5 DRG sections. The DRG sections were assessed using a light microscope (DM2500; Leica, Wetzlar, Germany), and equally sized (32000 μm^2) images were obtained. The number of DRG neurons in each image was manually counted using ImageJ software (National Institutes of Health, Bethesda, MD, USA). The number of DRG neurons per rat was then calculated as the mean number of L4 DRG neurons on the three images, the mean number of L5 DRG neurons on the three images, and the number of neurons in the L4 and L5 DRG of each rat shown as the number of neurons per 0.1 mm^2.

Reverse transcription quantitative polymerase chain reaction

The L4 and L5 DRG of each rat was dissected 7- and 14- days postoperative, and the L4 and L5 DRG of three intact rats were dissected as intact controls. Total RNA was extracted from DRG specimens using the RNeasy Plus Universal Mini Kit (Qiagen, Valencia, CA, USA), and RNA purity was determined by NanoDrop2000 (Thermo Fisher Scientific, Wilmington, DE, USA). The A260/A280 ratios of all specimens were > 1.98. Next, 1 μg of total RNA was reverse-transcribed to cDNA and RT-qPCR was performed using a 7500 Real-Time PCR System (Applied Biosystems, Foster City, CA, USA). TaqMan gene expression assays (Applied Biosystems) were used to detect nerve growth factor (NGF) (assay ID: Rn01533872_m1), BDNF (assay ID: Rn02531967_s1), neurotrophin-3 (NT-3)

147 (assay ID: Rn00579280_m1), growth-associated protein 43 (GAP-43) (assay ID:
148 Rn01474579_m1), interleukin 6 (IL-6) (assay ID: Rn01410330_m1), and tumor necrosis
149 factor (TNF) (assay ID: Rn99999017_m1).

150 Glyceraldehyde 3-phosphate dehydrogenase (GAPDH) (assay ID: Rn01775763_g1)
151 was chosen as the endogenous reference gene because of its high stability under the
152 experimental conditions. The data obtained were analyzed using the comparative
153 threshold cycle method, and the target gene expression was normalized to that of
154 GAPDH. The values of the calibration specimens (intact DRG specimens) were set to 1,
155 and the values of the specimens in the ultrasound and sham groups at each time point
156 post-injury are shown relative to those of the calibration specimens (Ito et al. 2020).

157

158 Immunohistochemistry

159 The DRG slides were washed with phosphate-buffered saline (PBS), blocked with
160 blocking buffer containing 5% goat serum (Jackson Immunoresearch, West Grove, PA,
161 USA), and incubated at room temperature for 30 min. Next, rabbit anti-BDNF (1:200; bs-
162 4989R, Bioss Inc., Woburn, MA, USA) primary antibody was added, and the slides were
163 incubated overnight at 4°C. The slides were then washed with PBS and incubated with
164 Alexa Fluor 488 goat anti-rabbit IgG (1:200; # A11008, Thermo Fisher Scientific)
165 secondary antibody at room temperature for 2 h. Finally, after washing with PBS,
166 coverslips were placed on all slides using an aqueous mounting medium.

167 One random cross-section of each DRG was viewed using a confocal laser scanning

168 microscope (FV10i; Olympus, Tokyo, Japan). For the semiquantitative analysis, the
169 appropriate laser intensity and sensitivity were set in the negative and positive control
170 sections, and all sections were processed under the same conditions. ImageJ software
171 was used to measure the mean gray values for the statistical analysis.
172
173 ## Kinematic analysis
174 Based on our previous research (Wang et al. 2018), a 3D motion analysis system
175 consisting of a treadmill, four 120-Hz-charged coupled device cameras, and data
176 processing software (Kinema Tracer System; Kissei Comtec, Nagano, Japan) was used for
177 the kinematic analysis. After the rats were anesthetized with 2% isoflurane, colored
178 hemispheric markers were attached to bilateral landmarks on the shaved skin as follows:
179 anterior superior iliac spine, greater trochanter, knee joint, lateral malleolus, and fifth
180 metatarsophalangeal joint. Both fourth toes were marked with pink ink. After the rats
181 recovered from the anesthesia, they walked on a treadmill at a speed of 12m/min, and
182 ten consecutive steps were recorded using four motion capture cameras. Here, we
183 analyzed the ankle angle and toe angle in the toe-off phase, which is the phase where
184 the foot loses its last contact with the ground. The ankle angle is defined as the angle
185 formed by the connecting line between the knee joint and the lateral malleolus, the
186 connecting line between the lateral malleolus and the fifth metatarsophalangeal joint
187 (angle between the two red lines in Fig. 5A). The toe angle is defined as the angle formed
188 by the extension line from the lateral malleolus to the fifth metatarsophalangeal joint,

the connecting line between the fifth metatarsophalangeal joint and the tip of the fourth toe (angle between the yellow line and the dashed line in Fig. 5A). Using data processing software, the 10-step ankle angles and toe angles in the toe-off phases were measured using marks on the rats, and the mean values of the ankle and toe angles were calculated (Wang et al. 2018).

Axon regeneration evaluation

Twenty-one days after surgery, a 5-mm-long sciatic nerve specimen was dissected from the epineural stitch after the animals were euthanized. The specimens were immersed in 1.44% paraformaldehyde and 1% glutaraldehyde in 0.036 M phosphate buffer (pH = 6.8) at 4°C overnight and fixed with 1% osmium tetroxide in 0.1 M phosphate buffer for 120 min. Subsequently, the specimens were dehydrated using graded ethanol and embedded in EPON (Luveak; Nacalai Tesque, Kyoto, Japan). Transverse sections (1-µm-thick) 5 mm distal to the injury site were prepared and stained with toluidine blue solution, and the cross-sections were viewed under a light microscope (Eclipse 80i; Nikon, Tokyo, Japan). According to a previous study (Ito et al. 2020), myelinated fiber density was counted in random areas of 90,000 mm^2 of one cross-section per rat using ImageJ, accounting for at least 30% of the total area of the image. The results are expressed as myelinated fiber density (fibers/mm^2).

Ultrathin transverse sections of the same tissue stained with uranyl acetate and lead citrate were viewed using a transmission electron microscope (Model H-7000; Hitachi

High-Technologies, Tokyo, Japan). According to a previous study (Wang et al. 2021), ten random pictures of each cross-section were obtained at 2000× magnification, and the shortest diameter of myelinated nerve fiber (a) and axon diameter (b) were measured using ImageJ. The myelin sheath thickness (c) of each myelinated nerve fiber was calculated using the formula (a–b)/2. The averages of these three parameters (a, b, and c) of each cross-section were considered the mean myelinated nerve diameter, mean axon diameter, and myelin sheath thickness, respectively.

Statistical analysis

All statistical analyses were performed using JMP Pro 15 software (SAS Institute, Cary, NC, USA). Data are expressed as mean ± standard deviation. The differences between the ultrasound and sham groups were evaluated using the Student's t-test, while those among the ultrasound, sham, and intact groups were evaluated using Tukey's honest significant differences test. Statistical significance was set at $p < 0.05$.

Results

No decrease in DRG neuron count was found at 14 days post-injury

A representative image of the DRG neurons is shown in Figure 2A. The quantitative analysis showed that the mean number of DRG neurons was not significantly different between the ultrasound and sham groups on day 14 (101 ± 10.91 vs. 89 ± 8.99, respectively; $p = 0.1035$) (Fig. 2B). There were no significant differences among the intact,

ultrasound, or sham groups at 14 days post-injury (Fig. 2B).

Ultrasound decreased *BDNF* and IL-6 mRNA expression in DRG at seven days post-injury

Compared with the intact group, *NGF, GAP-43,* and *IL-6* mRNA expressions in the DRG of the ultrasound and sham groups were significantly upregulated at 7 and 14 days post-injury (Figs. 3A, 3D, 3E), and the *BDNF* mRNA expression in the ultrasound and sham groups was significantly upregulated seven days post-injury (Fig. 3B). The BDNF levels did not differ between the calibration samples and the ultrasound or sham groups in terms of gene expression at 14 days post-injury (Fig. 3B). The gene expressions of *NT-3* and *TNF* at any time point were not significantly different between the groups and the calibration samples (Figs. 3C, 3F).

Compared with the sham group, our results indicated that the *BDNF* mRNA expressions of DRG in the ultrasound group were significantly downregulated at seven days post-injury (p = 0.0245) (Fig. 3B). The *IL-6* mRNA expression of the DRG in the ultrasound group were significantly suppressed compared to those in the sham group seven days post-injury (p = 0.0323) (Fig. 3E). The gene expressions of *BDNF* and *IL-6* at day 14 post-injury was not significantly different between the ultrasound and sham groups (Figs. 3B, 3E).

BDNF protein expression in the ultrasound group was higher in the

DRG 14 days post-injury

Representative images of DRG BDNF protein expression in the ultrasound and sham groups are shown in Figure 4A. No significant difference was found between the ultrasound and sham groups in the mean gray value of BDNF protein expression at seven days post-injury (44.54 ± 7.55 vs. 42.60 ± 4.23, respectively; $p = 0.6335$) (Fig. 4B). At the 14-day time point, the mean gray value of BDNF protein expression was significantly greater in the ultrasound group than in the sham group (21.44 ± 2.23 vs. 17.00 ± 2.86, respectively; $p = 0.0257$) (Fig. 4B).

Ultrasound promoted motor function recovery

A representative image of the ankle and toe angles in the toe-off phase is shown in Figure 5A. The ankle angle is between the two red lines, and the toe angle is between the yellow and dashed lines (Fig. 5A). The kinematic analysis results are shown in Figure 5B. Twenty-one days post-injury, the kinematic analysis showed that the toe angle in the toe-off phase was significantly larger in the ultrasound group than in the sham group (38.24 ± 6.55° vs. 30.72 ± 6.66°, respectively; $p = 0.0222$) (Fig. 5B). There was no significant difference in the ankle angles between the ultrasound and sham groups (94.73 ± 7.23° vs. 94.74 ± 14.69°, respectively; $p = 0.9992$) (Fig. 5B).

Ultrasound promoted sciatic nerve regeneration

Representative images of nerve fibers processed with toluidine blue staining are shown

in Figure 6A. Quantitative analysis indicated that the myelinated nerve fiber density was significantly higher in the ultrasound group than in the sham group at 21 days post-injury (7111 ± 629.04 vs. 5370 ± 743.53, respectively; $p = 0.0002$) (Fig. 6B).

Representative images of the transected sciatic nerve sections observed under transmission electron microscopy are shown in Figure 7A. A quantitative analysis showed that the myelin sheath thickness was significantly greater in the ultrasound group than in the sham group at 21 days post-injury (0.52 µm ± 0.04 vs. 0.46 µm ± 0.03, respectively; $p = 0.0077$) (Fig. 7B). However, the myelinated nerve and the axon diameters did not differ significantly between the ultrasound and sham groups at the 21-day time point (myelinated nerve diameter: 3.18 ± 0.18 vs. 3.18 ± 0.21 respectively; $p = 0.9837$; axon diameter: 2.14 ± 0.14 vs. 2.26 ± 0.17, respectively; $p = 0.1581$) (Fig. 7B).

Discussion

Ultrasound therapy is a noninvasive treatment that promotes peripheral nerve regeneration whose effectiveness has been proven in many studies (Ni et al. 2017; Ito et al. 2020; Wang et al. 2021; Kawai et al. 2022). Although many studies have verified the effects of ultrasound on injured sites, few have focused on its impact on the upstream neurons. Here we investigated the effects of ultrasound on DRG neurons in a rat sciatic nerve crush injury model.

Neurotrophic factors are secreted after PNI that can promote nerve regeneration (Menorca et al. 2013; Skaper 2018). A previous study showed that the mRNA expression

of *BDNF* in the DRG was upregulated in response to neuronal injury (Shen et al. 2020). Therefore, here we investigated the mRNA expression of neurotrophic factors in the DRG to explore the effect of ultrasound on the DRG after PNI. Previous studies reported that the mRNA expression of *NGF* and *BDNF* in the DRG was upregulated one day after a nerve injury, *NGF* mRNA expression levels remained high after 4 and 7 days, and *BDNF* mRNA expression levels returned to normal after four days (Shen et al. 2020). Consistent with the change trends of neurotrophic factors in a previous study (Shen et al. 2020), we found an increase in *NGF* mRNA expression 7 and 14 days post-injury in each group, and the *BDNF* mRNA expression level returned to normal earlier than the *NGF* mRNA expression. Additionally, in our study, *BDNF* mRNA expression in the DRG was significantly lower in the ultrasound group than in the sham group at seven days post-injury, but there was no significant difference between them at 14 days post-injury. In contrast, in the ultrasound group, BDNF protein expression in the DRG was significantly greater than that in the sham group at 14 days post-injury. Because of the BDNF retrograde axonal transport mechanism (DiStefano et al. 1992; Curtis et al. 1998), we speculate that this result may be due to the continuous promotion of the retrograde axonal transport of BDNF in neurons and acceleration of its accumulation in the DRG after a sciatic nerve crush injury. We considered that ultrasound therapy to the injured site promoted nerve regeneration, while the reaction process to the injury in DRG also converged at an early stage.

We found no intergroup differences in *NT-3* mRNA expression in the DRG of the

315 ultrasound, sham, or intact groups. This result indicates that *NT-3* expression in the DRG
316 may not be affected by sciatic nerve crush injury and may not respond to ultrasound
317 therapy. NT-3 reportedly affects neuronal survival and differentiation (Ventimiglia R et al.
318 1995) and can prevent re-myelination (Chan JR et al. 2001). Therefore, to promote re-
319 myelination after PNI, the mRNA expression of *NT-3* in DRG may not be upregulated,
320 which is consistent with previous results of the sciatic nerve (Funakoshi H et al. 1993; Ito
321 et al. 2020).

322 We found that *BDNF* mRNA expression in the DRG was significantly lower in the
323 ultrasound group than in the sham group seven days after the sciatic nerve crush injury,
324 which is contrary to the results of Ni et al. (2017). Perhaps the model used by Ni et al.
325 (2017) was more impaired than ours, had long-term re-positive reactions continuing in
326 the DRG, and featured *BDNF* mRNA expression that continued to increase for a longer
327 period. In this study, *BDNF* mRNA expression in the DRG stabilized to normal at 14 days
328 post-injury, which may indicate that the reaction of *BDNF* mRNA in the DRG was already
329 completed.

330 Levels of GAP-43, a membrane protein that participates in neuronal development
331 and plasticity, were increased in DRG after PNI (Woolf et al. 1990; Sommervaille et al.
332 1991). Because GAP-43 expression is correlated with axonal growth, it is usually used as
333 a marker of neuronal regeneration (Verge et al. 1990). There is evidence that *GAP-43*
334 mRNA expression in the DRG increases after PNI (Anderson et al. 2003), consistent with
335 our results. Our study results showed no difference in *GAP-43* mRNA expression

between the ultrasound and sham groups at any time point post-injury, indicating that ultrasound did not promote an increase in *GAP-43* mRNA expression in the DRG after PNI.

Pro-inflammatory factors such as TNF and IL-6 are rapidly expressed in the distal stump after PNI (Bosse 2012). An early-stage (within hours) increase in TNF expression may control phospholipase-A2 expression and activation in Schwann cells and macrophages, thereby promoting the initiation of myelin breakdown and the progression of Wallerian degeneration after PNI (Ribardo et al. 2001; Gaudet et al. 2011). Early IL-6 expression can increase the expression of regeneration-associated genes in neurons to promote axonal growth (Cafferty et al. 2004; Cao et al. 2006). However, intense inflammatory responses may not be conducive to post-PNI recovery (Tang et al. 2018). To clarify the effect of ultrasound on the mRNA expression of pro-inflammatory factors in DRG, we investigated the mRNA expression of pro-inflammatory factors (TNF and IL-6) at 7 and 14 days post-injury. We found that *IL-6* mRNA expression at 7 and 14 days post-injury increased by hundreds of times in each group versus that in intact rats. Compared to the sham group, the *IL-6* mRNA expression of DRG in the ultrasound group was significantly reduced at seven days post-injury. Our previous study also indicated that ultrasound therapy suppressed *IL-6* mRNA expression of the distal stump of the sciatic nerve seven days after PNI (Ito et al. 2020). These results suggest that ultrasound therapy may accelerate the early inflammation after PNI. However, in the present study, we did not observe any significant change in *TNF* mRNA expression in the DRG, although

357 significantly higher expression was observed in the sciatic nerves seven days after PNI in
358 our previous study (Ito et al. 2020). This result indicates that *TNF* expression in the DRG
359 was not affected by sciatic nerve crush injury and did not respond to ultrasound therapy.
360 Our previous research showed that the ankle and toe angles in the toe-off phase
361 were significantly decreased after sciatic nerve crush injury in rats and that the increases
362 in the ankle and toe angles in the toe-off phase were highly correlated with nerve
363 regeneration (Wang et al. 2018; Wang et al. 2021; Kawai et al. 2022). In this study,
364 although there was no difference in the ankle angles in the toe-off phase at 21 days post-
365 injury, the mean toe angle of the ultrasound group was significantly recovered compared
366 to that of the sham group, a finding that is consistent with our previous results (Wang et
367 al. 2021). Consistent with our previous studies (Wang et al. 2021; Kawai et al. 2022), we
368 found that the myelinated fiber density and myelin sheath thickness in the ultrasound
369 group were significantly greater than those in the sham group at 21 days post-injury.
370 These results confirm the effect of ultrasound on motor function recovery and nerve
371 regeneration after sciatic nerve crush injury in a rat model.
372 This study had several limitations. First, we analyzed mRNA expression in the DRG at
373 only 7 and 14 days post-injury. To further study the effect of ultrasound on upstream
374 dynamic changes in neurotrophic factor mRNA expression after injury, earlier time points
375 for mRNA expression experiments should be examined. We also found that ultrasound
376 therapy of the injured site affects gene and protein expressions in the DRG after PNI;
377 however, the association between these changes and the promotion of nerve

regeneration remains unclear. Further studies are needed to investigate the association between the effect of ultrasound therapy on gene and protein expression and the promotion of nerve regeneration in the PNI model. Third, unlike a previous study (West et al. 2007), we found no significant reduction in DRG neuron counts post-injury, which may be because our sciatic nerve injury model was insufficient to cause a significant decrease in DRG neuron counts. As there was no significant cell loss in the DRG, the neuroprotective effect of ultrasound therapy could not be verified in this study. Therefore, other nerve injury models should be used to study the neuroprotective effects of ultrasound therapy. Finally, because the sciatic nerve contains motor and sensory fibers, we did not evaluate the sensory function of the sciatic nerve crush injury model in this study. Further studies are needed to investigate the recovery of sensory function after PNI.

Conclusion

Here we investigated the effects of ultrasound therapy on the DRG in a rat model of sciatic nerve crush injury. We confirmed the effect of ultrasound therapy at the injury site on nerve regeneration. We found that, after ultrasound therapy, the mRNA expressions of *BDNF* and *IL-6* were reduced in the DRG on day seven and the protein expression of BDNF was maintained at a higher level in the DRG on day 14. This shows meaning that ultrasound therapy on the injury site can modulate the gene and protein expressions in the DRG in a sciatic nerve crush injury rat model.

Acknowledgements

This work was supported by JSPS KAKENHI grants (JP18H03129 and JP21K19709). We thank Keiko Okamoto Furuta and Haruyasu Kouda (Division of Electron Microscopic Study, Center for Anatomical Studies, Graduate School of Medicine, Kyoto University) for their technical assistance with the electron microscopy. We also thank Editage (www.editage.com) for the English language editing.

Conflict of Interest Statement

The authors have no conflicts of interest to declare.

References

Anderson KD, Merhege MA, Morin M, Bolognani F, Perrone-Bizzozero NI. Increased expression and localization of the RNA-binding protein HuD and GAP-43 mRNA to cytoplasmic granules in DRG neurons during nerve regeneration. Exp Neurol 2003;183:100-108.

Bosse F. Extrinsic cellular and molecular mediators of peripheral axonal regeneration. Cell Tissue Res 2012;349:5-14.

Cafferty WB, Gardiner NJ, Das P, Qiu J, McMahon SB, Thompson SW. Conditioning injury-induced spinal axon regeneration fails in interleukin-6 knock-out mice. J Neurosci 2004;24:4432-4443.

Cao Z, Gao Y, Bryson JB, Hou J, Chaudhry N, Siddiq M, Martinez J, Spencer T, Carmel J, Hart RB, Filbin MT. The cytokine interleukin-6 is sufficient but not necessary to mimic the peripheral conditioning lesion effect on axonal growth. J Neuronsci 2006;26:5565-5573.

Chan JR, Cosgaya JM, Wu YJ, Shooter EM. Neurotrophins are key mediators of the myelination program in the peripheral nervous system. Proc Natl Acad Sci U S A 2001;98:14661-14668.

Chen WZ, Qiao H, Zhou W, Wu J, Wang ZB. Upgraded nerve growth factor expression induced by low-intensity continuous-wave ultrasound accelerates regeneration of neurotometicly injured sciatic nerve in rats. Ultrasound Med Biol 2010;36:1109-1117.

Curtis R, Tonra JR, Stark JL, Adryan KM, Park JS, Cliffer KD, Lindsay RM, DiStefano PS. Neuronal injury increases retrograde axonal transport of the neurotrophins to spinal sensory neurons and motor neurons via multiple receptor mechanisms. Mol Cell Neurosci 1998;12:105-118.

DeFrancesco-Lisowitz A, Lindborg JA, Niemi JP, Zigmond RE. The neuroimmunology of degeneration and regeneration in the peripheral nervous system. Neuroscience 2015;302:174-203.

Deumens R, Bozkurt A, Meek MF, Marcus MA, Joosten EA, Weis J, Brook GA. Repairing injured peripheral nerves: Bridging the gap. Prog Neurobiol 2010;92:245-276.

DiStefano PS, Friedman B, Radziejewski C, Alexander C, Boland P, Schick CM, Lindsay RM,

441 Wiegand SJ. The neurotrophins BDNF, NT-3, and NGF display distinct patterns of
442 retrograde axonal transport in peripheral and central neurons. Neuron 1992;8:983-
443 993.
444 Funakoshi H, Frisén J, Barbany G, Timmusk T, Zachrisson O, Verge VM, Persson H.
445 Differential expression of mRNAs for neurotrophins and their receptors after
446 axotomy of the sciatic nerve. J Cell Biol 1993;123:455-465.
447 Gaudet AD, Popovich PG, Ramer MS. Wallerian degeneration: gaining perspective on
448 inflammatory events after peripheral nerve injury. J Neuroinflammation 2011;8:110.
449 Gordon T. Peripheral Nerve Regeneration and Muscle Reinnervation. Int J Mol Sci
450 2020;21:8652.
451 Ito A, Wang T, Nakahara R, Kawai H, Nishitani K, Aoyama T, Kuroki H. Ultrasound therapy
452 with optimal intensity facilitates peripheral nerve regeneration in rats through
453 suppression of pro-inflammatory and nerve growth inhibitor gene expression. PLoS
454 One 2020;15:e0234691.
455 Kawai H, Ito A, Wang T, Xu S, Kuroki H. Investigating the Optimal Initiation Time of
456 Ultrasound Therapy for Peripheral Nerve Regeneration after Axonotmesis in Rats.
457 Ultrasound Med Biol 2022;48:304-312.
458 Martini R, Fischer S, López-Vales R, David S. Interactions between Schwann cells and
459 macrophages in injury and inherited demyelinating disease. Glia 2008;56:1566-
460 1577.
461 Menorca RM, Fussell TS, Elfar JC. Nerve physiology: mechanisms of injury and recovery.

462 Hand Clin 2013;29:317-330.
463 Modrak M, Talukder MAH, Gurgenashvili K, Noble M, Elfar JC. Peripheral nerve injury and
464 myelination: Potential therapeutic strategies. J Neurosci Res 2020;98:780-795.
465 Ni XJ, Wang XD, Zhao YH, Sun HL, Hu YM, Yao J, Wang Y. The Effect of Low-Intensity
466 Ultrasound on Brain-Derived Neurotropic Factor Expression in a Rat Sciatic Nerve
467 Crushed Injury Model. Ultrasound Med Biol 2017;43:461-468.
468 Ribardo DA, Crowe SE, Kuhl KR, Peterson JW, Chopra AK. Prostaglandin levels in
469 stimulated macrophages are controlled by phospholipase A2-activating protein and
470 by activation of phospholipase C and D. J Biol Chem 2001;276:5467-5475.
471 Robinson LR. Traumatic injury to peripheral nerves. Muscle Nerve 2000;23:863-873.
472 Sanna MD, Ghelardini C, Galeotti N. HuD-mediated distinct BDNF regulatory pathways
473 promote regeneration after nerve injury. Brain Res 2017;1659:55-63.
474 Scheib J, Höke A. Advances in peripheral nerve regeneration. Nat Rev Neurol 2013;9:668-
475 676.
476 Seddon HJ. Three types of nerve injury. Brain 1943;66:237-288.
477 Shen YY, Gu XK, Zhang RR, Qian TM, Li SY, Yi S. Biological characteristics of dynamic
478 expression of nerve regeneration related growth factors in dorsal root ganglia after
479 peripheral nerve injury. Neural Regen Res 2020;15:1502-1509.
480 Skaper SD. Neurotrophic Factors: An Overview. Methods Mol Biol 2018;1727:1-17.
481 Sommervaille T, Reynolds ML, Woolf CJ. Time-dependent differences in the increase in
482 GAP-43 expression in dorsal root ganglion cells after peripheral axotomy.

Neuroscience 1991;45:213-220.

Song XY, Li F, Zhang FH, Zhong JH, Zhou XF. Peripherally-derived BDNF promotes regeneration of ascending sensory neurons after spinal cord injury. PLoS One 2008;3:e1707.

Tang G, Yao J, Shen R, Ji A, Ma K, Cong B, Wang F, Zhu L, Wang X, Ding Y, Zhang B. Reduced inflammatory factor expression facilitates recovery after sciatic nerve injury in TLR4 mutant mice. Int Immunopharmacol 2018;55:77-85.

Taylor CA, Braza D, Rice JB, Dillingham T. The incidence of peripheral nerve injury in extremity trauma. Am J Phys Med Rehabil 2008;87:381-385.

ter Haar G. Therapeutic applications of ultrasound. Prog Biophys Mol Biol 2007;93:111-129.

Ventimiglia R, Mather PE, Jones BE, Lindsay RM. The neurotrophins BDNF, NT-3 and NT-4/5 promote survival and morphological and biochemical differentiation of striatal neurons in vitro. Eur J Neurosci 1995;7:213-222.

Verge VM, Tetzlaff W, Richardson PM, Bisby MA. Correlation between GAP43 and nerve growth factor receptors in rat sensory neurons. J Neurosci 1990;10:926-934.

Wang T, Ito A, Aoyama T, Nakahara R, Nakahata A, Ji X, Zhang J, Kawai H, Kuroki H. Functional evaluation outcomes correlate with histomorphometric changes in the rat sciatic nerve crush injury model: A comparison between sciatic functional index and kinematic analysis. PLoS One 2018;13:e0208985.

Wang T, Ito A, Xu S, Kawai H, Kuroki H, Aoyama T. Low-Intensity Pulsed Ultrasound

Prompts Both Functional and Histologic Improvements While Upregulating the Brain-Derived Neurotrophic Factor Expression after Sciatic Crush Injury in Rats. Ultrasound Med Biol 2021;47:1586-1595.

West CA, Davies KA, Hart AM, Wiberg M, Williams SR, Terenghi G. Volumetric magnetic resonance imaging of dorsal root ganglia for the objective quantitative assessment of neuron death after peripheral nerve injury. Exp Neurol 2007;203:22-33.

Woolf CJ, Reynolds ML, Molander C, O'Brien C, Lindsay RM, Benowitz LI. The growth-associated protein GAP-43 appears in dorsal root ganglion cells and in the dorsal horn of the rat spinal cord following peripheral nerve injury. Neuroscience 1990;34:465-478.

Yang M, Rawson JL, Zhang EW, Arnold PB, Lineaweaver W, Zhang F. Comparisons of outcomes from repair of median nerve and ulnar nerve defect with nerve graft and tubulization: a meta-analysis. J Reconstr Microsurg 2011;27:451-460.

Figure Captions

Figure 1: Study design and ultrasound therapy

(A) Study design describing the analytical methods. (B) A representative image of the ultrasound therapy procedure.

Figure 2: Dorsal root ganglion neurons

(A) Representative image of dorsal root ganglion (DRG) neurons with hematoxylin and eosin staining. Scale bar: 10 µm. (B) Mean number of DRG neurons at 14 days post-injury. All data are shown as mean ± standard deviation (ultrasound and sham group: n = 5; intact group: n = 3).

Figure 3: Reverse transcription quantitative polymerase chain reaction

Gene expressions of (A) *NGF*, (B) *BDNF*, (C) *NT-3*, (D) *GAP-43*, (E) *IL-6*, and (F) *TNF* in the intact, sham, and ultrasound groups at 7 and 14 days post-injury. All data are shown as mean ± standard deviation. The mean value of the calibration samples (intact dorsal root ganglion specimens, n = 3) was set to 1 (*$p < 0.05$ vs. sham group; #$p < 0.05$, ##$p < 0.01$ vs. calibration samples, n = 9).

Figure. 4: Protein expression of brain-derived neurotrophic factor (BDNF) in dorsal root ganglion (DRG)

(A) Representative images of BDNF protein expression in the sham and ultrasound group.

Scale bar: 50 µm. (B) Mean gray value of DRG neurons. All data are shown as mean ± standard deviation (*$p < 0.05$, n = 5).

Figure. 5: Kinematic analysis

(A). Representative image of ankle angle (angle between the two red lines) and toe angle (angle between the yellow line and the dashed line) in toe-off phase. (B) Joint angle in the toe-off phase at 21 days post-injury. All data are shown as mean ± standard deviation (*$p < 0.05$, n = 8).

Figure 6: Myelinated fiber density

(A) Representative image of the sciatic nerve with toluidine blue staining. Scale bar: 100 µm. (B) Mean myelinated fiber density at 21 days post-injury. All data are shown as mean ± standard deviation (**$p < 0.01$, n = 8).

Figure. 7: Transmission electron micrographs of the sciatic nerve

(A) Representative transmission electron micrograph of a transected sciatic nerve in the sham and ultrasound groups at 21 days post-injury. Scale bar: 2 µm. (B) Mean myelinated nerve diameter. (C) Mean axon diameter. (D) Mean myelin sheath thickness. All data are shown as mean ± standard deviation (**$p < 0.01$, n = 8).

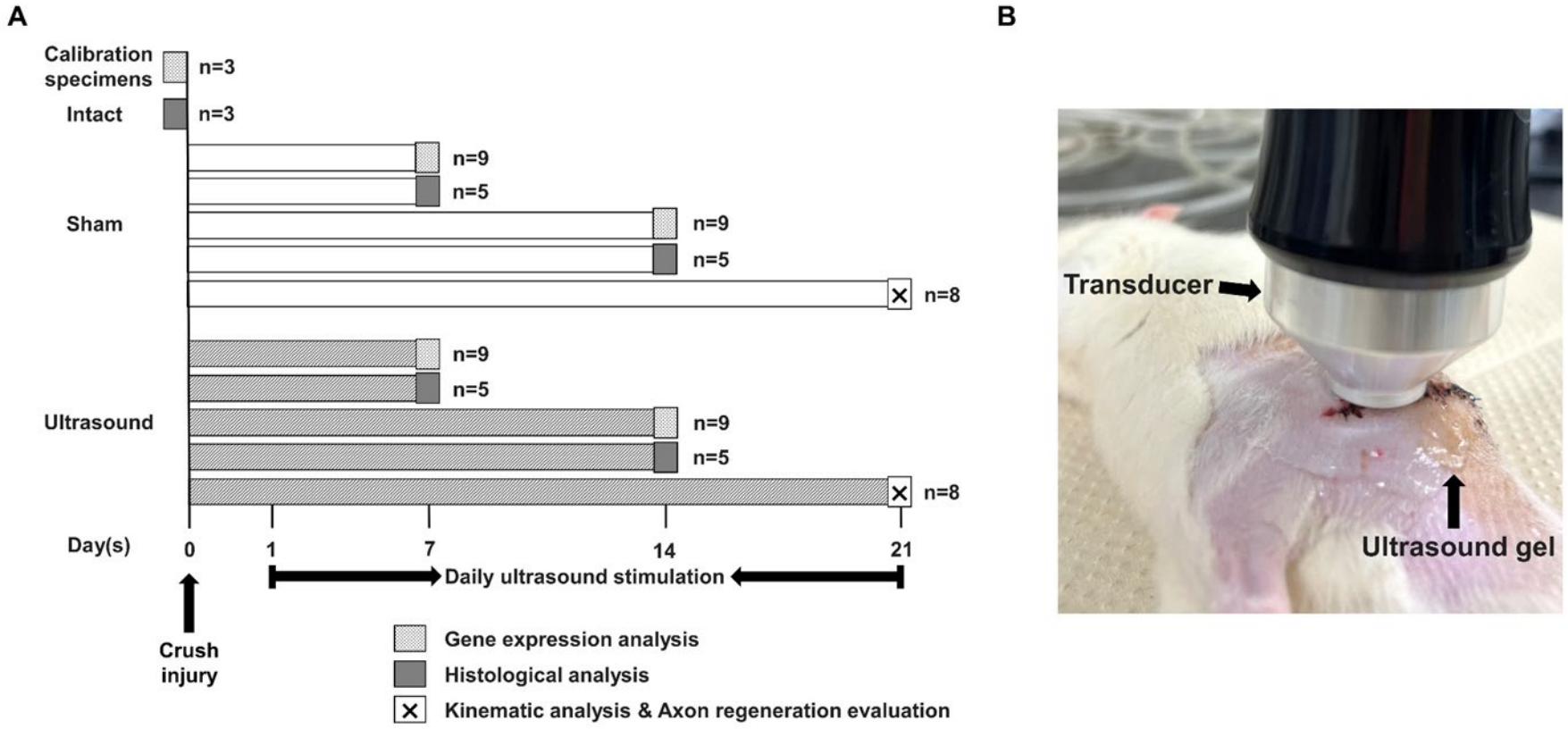

Figure 1: Study design and ultrasound therapy

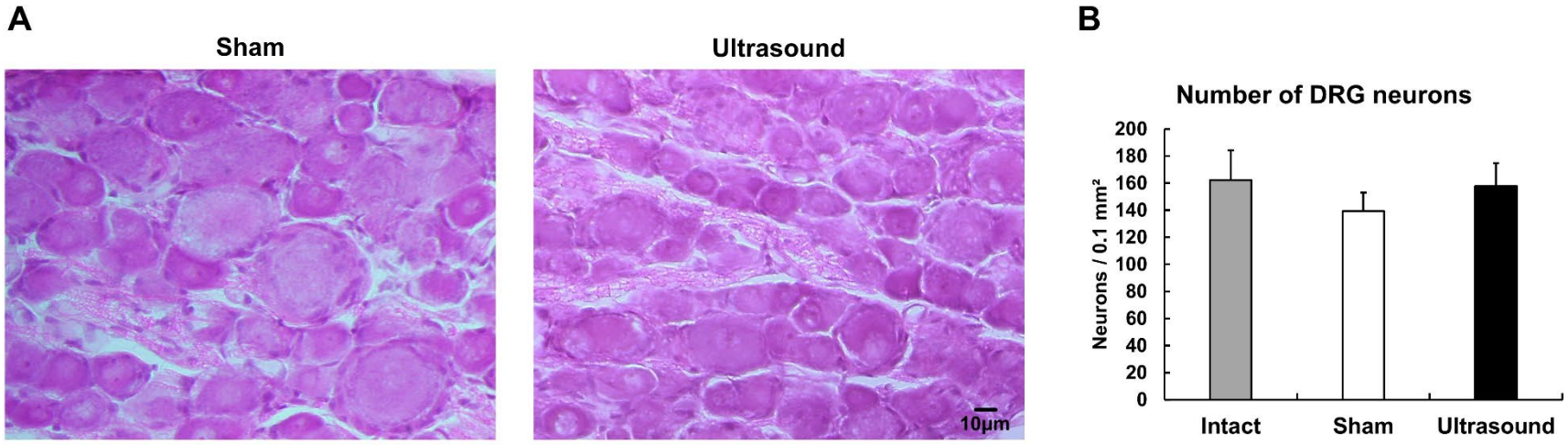

Figure 2: Dorsal root ganglion neurons

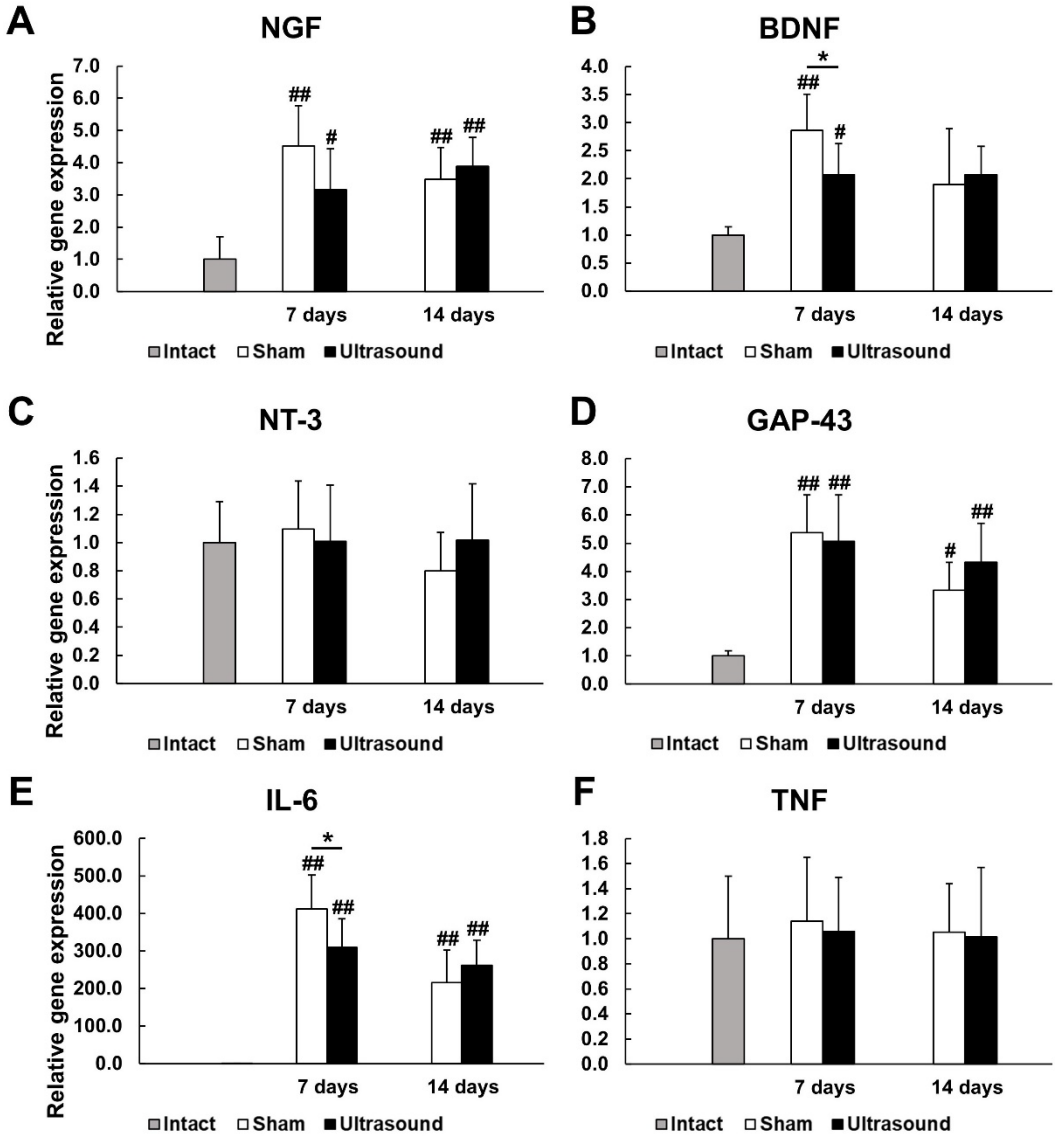

Figure 3: Reverse transcription quantitative polymerase chain reaction

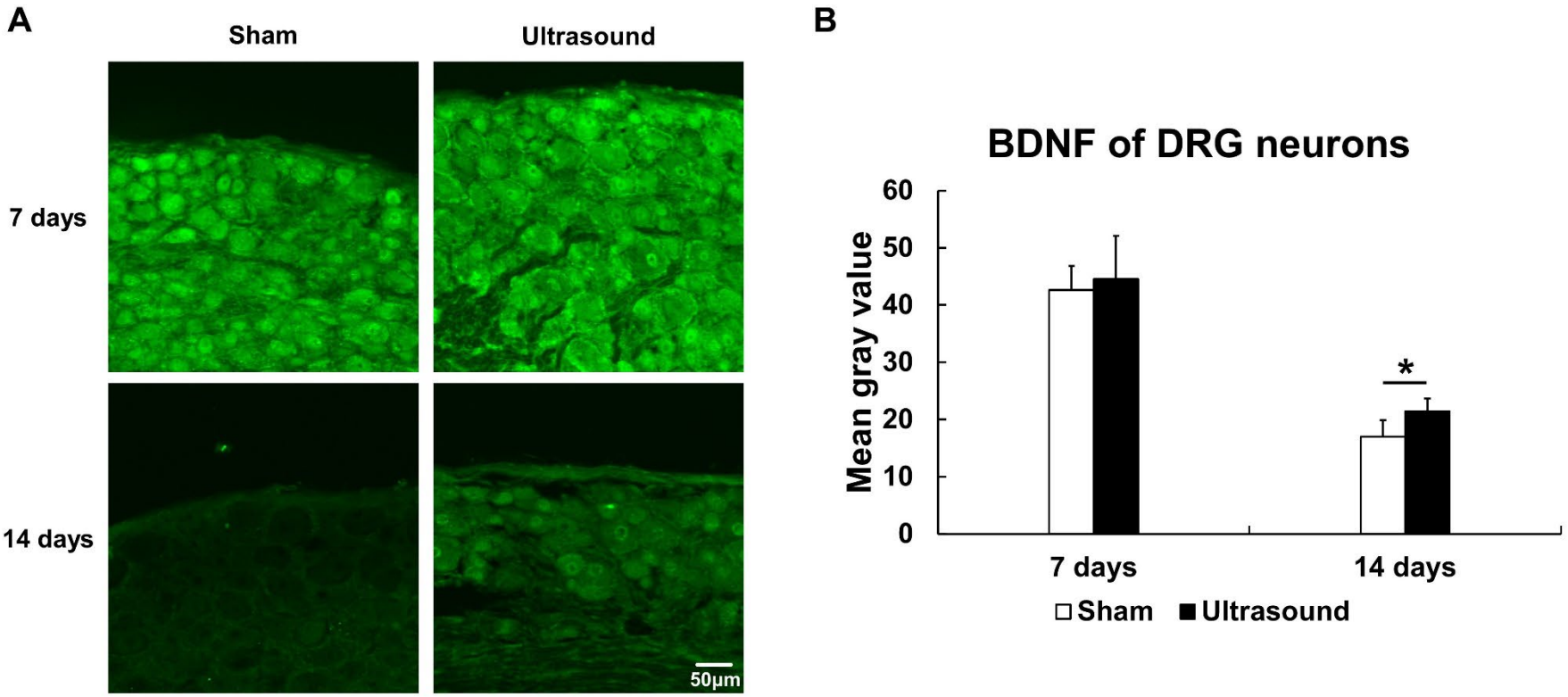

Figure. 4: Protein expression of brain-derived neurotrophic factor (BDNF) in dorsal root ganglion (DRG)

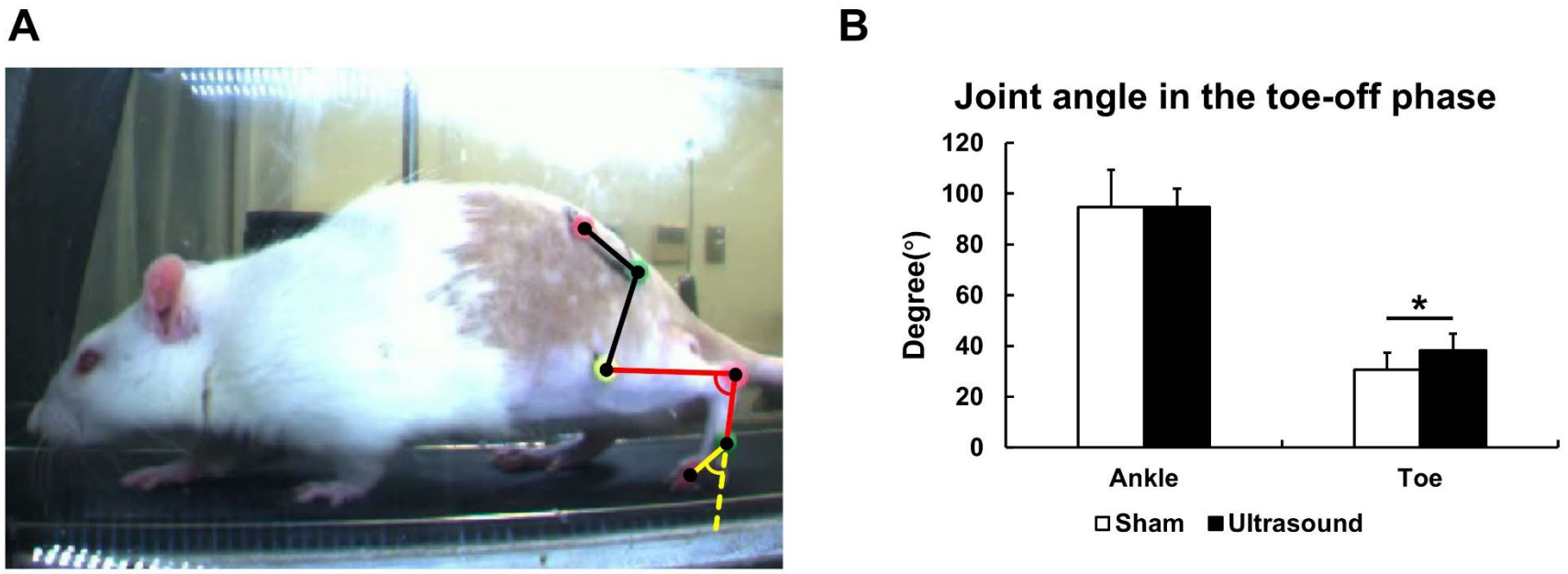

Figure. 5: Kinematic analysis

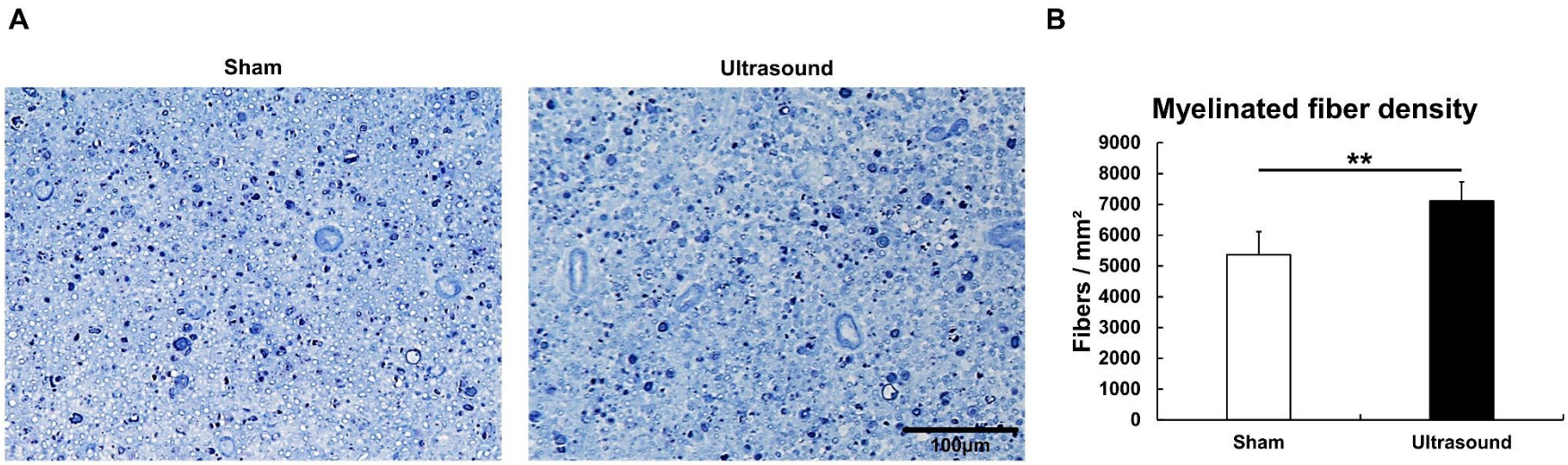

Figure 6: Myelinated fiber density

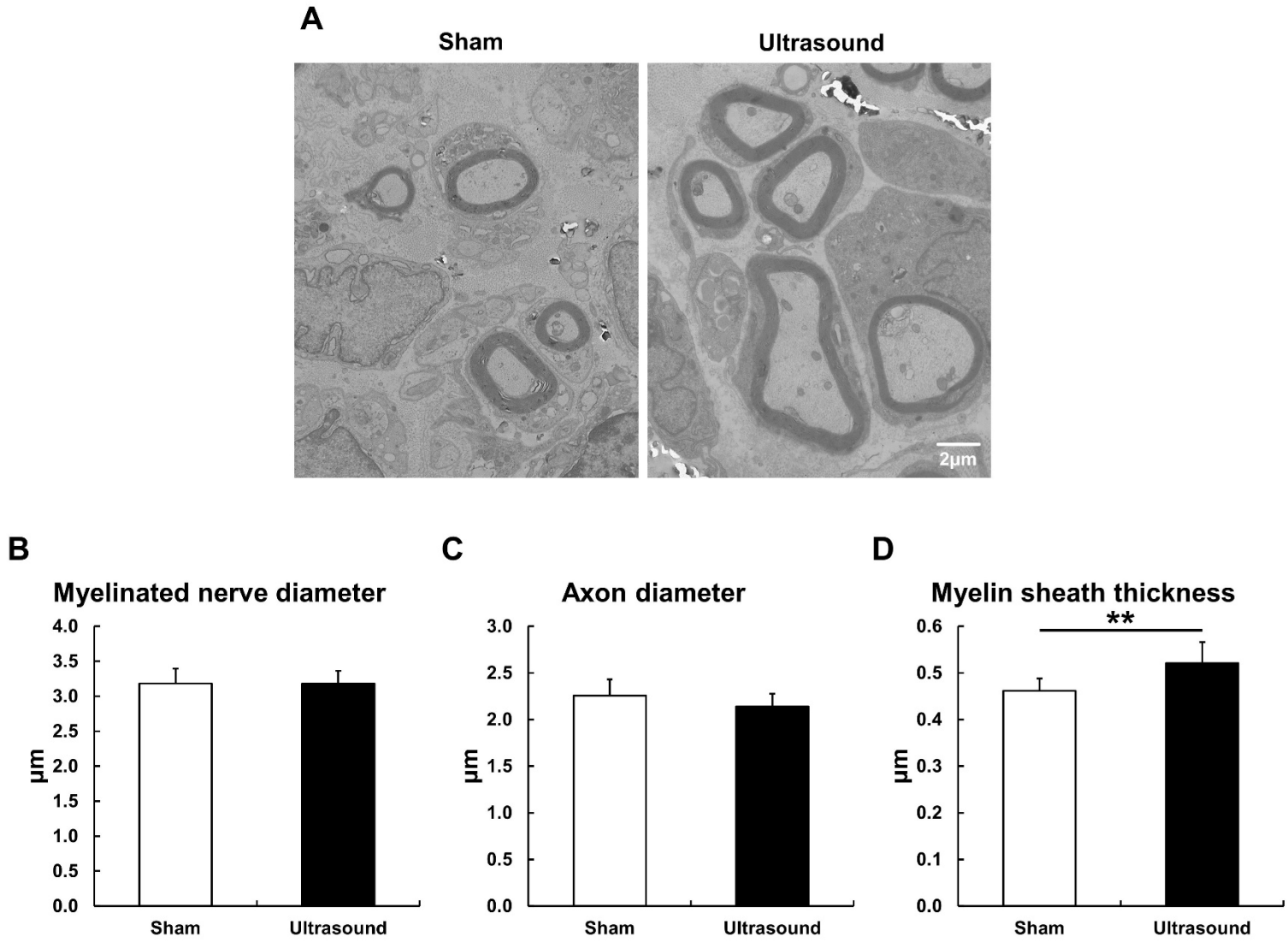

Figure. 7: Transmission electron micrographs of the sciatic nerve